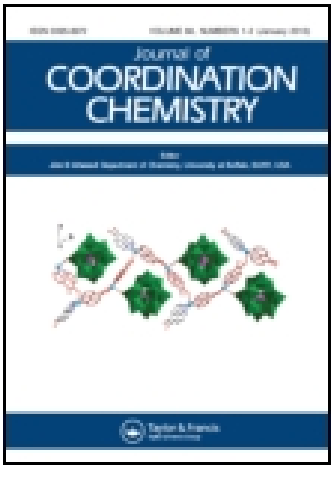

Journal of Coordination Chemistry
Publication details, including instructions for authors and subscription information:
http://www.tandfonline.com/loi/gcoo20

Construction of two lanthanide complexes based on N- and O-donors: synthesis, luminescence, and biological activities

Liang Qin[a], De-Yun Ma[a], Rong Deng[a] & Jun Xu[b]
[a] School of Chemistry and Chemical Engineering, Zhaoqing University, Zhaoqing, PR China
[b] College of Medicine, Jinan University, Guangzhou, PR China
Accepted author version posted online: 13 Mar 2014.Published online: 07 Apr 2014.

To cite this article: Liang Qin, De-Yun Ma, Rong Deng & Jun Xu (2014) Construction of two lanthanide complexes based on N- and O-donors: synthesis, luminescence, and biological activities, Journal of Coordination Chemistry, 67:6, 1032-1045, DOI: 10.1080/00958972.2014.904042

To link to this article: http://dx.doi.org/10.1080/00958972.2014.904042

Journal of Coordination Chemistry, 2014
Vol. 67, No. 6, 1032–1045, http://dx.doi.org/10.1080/00958972.2014.904042

Construction of two lanthanide complexes based on N- and O-donors: synthesis, luminescence, and biological activities

LIANG QIN*†, DE-YUN MA†, RONG DENG† and JUN XU*‡

†School of Chemistry and Chemical Engineering, Zhaoqing University, Zhaoqing, PR China
‡College of Medicine, Jinan University, Guangzhou, PR China

(*Received 2 May 2013; accepted 4 January 2014*)

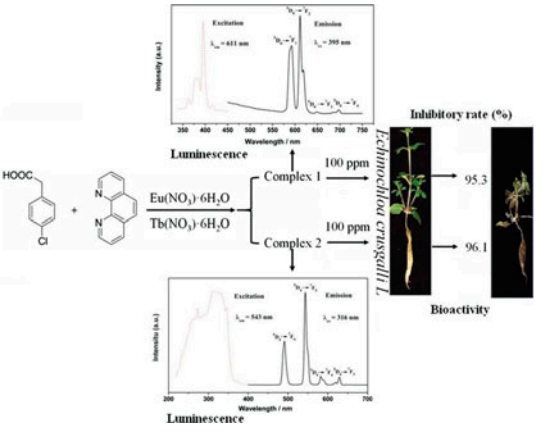

Two new isostructural dinuclear complexes, $Ln_2(4\text{-cpa})_6(phen)_2$ (Ln = Eu (**1**); Tb (**2**), 4-cpa^- = 4-chlorophenylacetate, phen = 1,10-phenanthroline), have been hydrothermally synthesized and characterized by IR spectroscopy, elemental analysis, thermogravimetric analysis, powder X-ray diffraction, and single-crystal X-ray diffraction. The lanthanides are bridged by two bidentate and two tridentate carboxylato groups to give centrosymmetric dimers with Ln···Ln separations of 3.967 (2) and 3.937(3) Å for **1** and **2**, respectively. Each metal is nine-coordinate and exhibits a distorted tricapped trigonal prismatic geometry. Both **1** and **2** emit characteristic, intense luminescence at room temperature with lifetimes up to 0.890 ms (at 611 nm) and 0.995 ms (at 543 nm). Poor luminescence efficiency is observed for **2**. 4-Chlorophenylacetate, **1** and **2** have been screened for their phytogrowth-inhibitory activities against *Brassica napus* L. and *Echinochloa crusgalli* L., and the results are compared with the activity of quizalofop-P-ethyl.

Keywords: Lanthanide complexes; Hydrothermal synthesis; Crystal structures; Luminescent properties; Biological activities

*Corresponding authors. Email: liangq@zqu.edu.cn (L. Qin); xujun@jnu.edu.cn (J. Xu)

1. Introduction

Lanthanide complexes have attracted attention in coordination chemistry because of their intriguing architectures and topologies and their potential applications as luminescent materials and probes, magnetic materials, catalysts, porous materials, and biological materials [1–8]. Although the high and variable coordination numbers and flexible coordination environments of lanthanide ions may create complications in controlling reactions and thereby the final structures of the products, the fascinating coordination chemistry and the rich structural properties along with applications of lanthanide complexes have attracted interest [9–12].

Aromatic carboxylic acids, with versatile coordination, are widely employed in the construction of luminescent lanthanide coordination polymers, which usually exhibit high thermal stability and intense fluorescence because of a large conjugated π-electron system [13]. We are interested in the coordination chemistry of 4-chlorophenylacetic acid (4-Hcpa), a flexible ligand with versatile binding and coordination, which can be an excellent candidate for the construction of lanthanide coordination polymers [14, 15]. So far, however, construction of lanthanide complexes based on 4-cpa$^-$ has not been reported.

In this article, we present our attempts to generate via hydrothermal routes lanthanide complexes from 4-Hcpa and 1,10-phenanthroline (phen). We report the formation, structure, and properties of two new, isostructural, dinuclear complexes $Ln_2(4\text{-cpa})_6(phen)_2$ (Ln = Eu (**1**); Tb (**2**)).

2. Experimental

2.1. *General materials and method*

All chemicals were obtained from commercial sources and used as received. C, H, and N elemental analyses were carried out with a Vario EL III Elemental Analyzer. Infrared spectra were recorded (4000–400 cm^{-1}) as KBr disks on a Shimadzu IR-440 spectrometer. Thermogravimetric analyses (TGA) were performed on an automatic simultaneous thermal analyzer (DTG-60, Shimadzu) between ambient temperature and 800 °C under a flow of N_2 at a heating rate of 10 °C/min. Luminescence spectra and lifetimes for crystalline samples were recorded at room temperature on an Edinburgh FLS920 phosphorimeter. The overall absolute quantum yields ($\Phi_{overall}$) of **2** were measured using an integrating sphere in a Combined Fluorescence Lifetime and Steady State Spectrometer (FLSP920). The PL quantum yields of thin films ($\Phi_{overall}$) were determined using a calibrated integrating sphere system. A Xe-arc lamp was used to excite the thin-film samples that were placed in the sphere. The samples were prepared by drop casting the material placed between two quartz coverslips. The quantum yields were determined by comparing the spectral intensities of the lamp and the sample emission as reported in the literature [16]. Using this experimental setup and the integrating sphere system, the solid-state fluorescence quantum yield of a thin film of the standard green OLED material tris-8-hydroxyquinolinolato aluminum was determined to be 0.18, which is consistent with previously reported values [17]. The sample was measured several times under slightly different experimental conditions. The estimated error for the quantum yields is ±10% [18].

2.2. *Biological activity test*

The herbicidal activities of 4-Hcpa, **1** and **2** were determined using *Brassica napus* L. and *Echinochloa crusgalli* L. as samples of dicotyledonous and monocotyledonous plants, respectively [19, 20]. Solutions of the tested compounds were prepared by dissolving them in DMSO (100 μL) with the addition of Tween 20 (2 μL) and then diluting with distilled water. The germinated seeds were placed on two filter papers in a 9-cm Petri plate, to which 5 mL of the tested solution was added in advance. Usually, 15 seeds were used on each plate. The plates were placed in a dark room and allowed to germinate for 72 h at 25 °C. The lengths of 10 seed roots selected from each plate were measured and the means were calculated. Quizalofop-p-ethyl, a commercial aryloxy-phenoxy propionate herbicide, and an emulsion which did not contain any tested compounds were used as control and blank, respectively. For all of the bioassay tests, each treatment was repeated thrice. The inhibitory rate was calculated relative to the blank.

2.3. *Preparation of compounds*

2.3.1. $Eu_2(4\text{-cpa})_6(phen)_2$ (1). $Eu(NO_3)_3{\cdot}6H_2O$ (0.223 g, 0.5 mM), 4-Hcpa (0.085 g, 0.5 mM), phen (0.09 g, 0.5 mM), and distilled water (15 mL) were heated to 160 °C for 54 h in a 23 mL stainless steel reactor with a Teflon liner, followed by slow cooling to room temperature. The resulting reaction produced red, block-shaped crystals (0.27 g, 64% yield based on 4-Hcpa) that were washed with alcohol to give pure samples. Elem. Anal. Calcd (%) for $C_{72}H_{52}Cl_6Eu_2N_4O_{12}$: C, 51.37; H, 3.09; N, 3.33. Found: C, 51.34; H, 3.12; N, 3.37. IR (cm^{-1}): 3076(w), 1609(vs), 1560(m), 1493(s), 1437(w), 1409(w), 1393(w), 1293 (m), 1244(w), 1215(w), 1085(m), 1013(m), 865(w), 845(m), 809(m), 769(w), 729(m), 681 (w), 637(w), 501(w), 473(w), 421(m).

2.3.2. $Tb_2(4\text{-cpa})_6(phen)_2$ (2). Complex **2** was prepared by the same procedure as **1** except that $Eu(NO_3)_3{\cdot}6H_2O$ was replaced by $Tb(NO_3)_3{\cdot}6H_2O$ (0.25 g, 60% yield based on 4-Hcpa). Elem. Anal. Calcd (%) for $C_{72}H_{52}Cl_6Tb_2N_4O_{12}$: C, 50.95; H, 3.07; N, 3.30. Found: C, 50.90; H, 3.09; N, 3.34. IR (cm^{-1}): 3080(m), 1611(vs), 1557(m), 1492(s), 1429 (s), 1405(s), 1345(m), 1289(s), 1233(w), 1197 (m), 1149(m), 1089(s), 1013(m), 925(m), 865(w), 845(s), 805(m), 765(w), 729(s), 673(m), 637(w), 593(w), 501(m), 473(w), 413(w).

2.4. *X-ray crystallography*

X-ray diffractions for **1** and **2** were performed on a Bruker Smart Apex II CCD diffractometer operating at 50 kV and 30 mA using MoKα radiation ($\lambda = 0.71073$ Å) at room temperature. Data collection and reduction were performed using the APEX II software [21]. Multi-scan absorption corrections were applied for all the data-sets with APEX II [21]. Small residual absorption effects were treated with XABS2 [22]. Both structures were solved by direct methods and refined by least-squares against F^2 using the SHELXTL program package [23]. All non-hydrogen atoms were refined with anisotropic displacement parameters. Hydrogens attached to carbon were placed in geometrically idealized positions and refined using a riding model. Crystallographic data and refinement parameters for **1** and **2** are listed in table 1. Selected bond lengths and angles for **1** and **2** are given in table 2.

Table 1. Crystallographic data and refinement parameters for **1** and **2**.

Compound	**1**	**2**
Empirical formula	$C_{72}H_{52}Cl_6Eu_2N_4O_{12}$	$C_{72}H_{52}Cl_6Tb_2N_4O_{12}$
Formula weight	1681.80	1695.72
Temperature (K)	296(2)	296(2)
Crystal system	Triclinic	Triclinic
Space group	*P-1*	*P-1*
a (Å)	10.6697(6)	10.6474(6)
b (Å)	12.5862(7)	12.5435(7)
c (Å)	13.3012(7)	13.3632(7)
α (°)	102.7030(10)	102.8200(10)
β (°)	97.8140(10)	97.7400(10)
γ (°)	91.9770(10)	91.9400(10)
V (Å^3)	1722.49(16)	1720.63(16)
Z, *D* (Mg m^3)	1, 1.621	1, 1.636
Reflections collected/unique	18,027/6117	19,044/6138
θ (°)	2.55–25.20	1.58–25.20
Goodness-of-fit on F^2	1.146	1.096
$R(I > 2\sigma)$	$R_1 = 0.0271$	$R_1 = 0.0274$
	$wR_2 = 0.0837$	$wR_2 = 0.0846$
R (all data)	$R_1 = 0.0354$	$R_1 = 0.0353$
	$wR_2 = 0.1261$	$wR_2 = 0.1192$
Largest diff. peak and hole (Å^{-3})	1.058 and −1.040	0.802 and −0.987

$R = \sum(||F_o| - |F_c||)/\sum|F_o|$; $wR = [\sum w(F_o^2 - F_c^2)^2/\sum w(F_o)^2]^{1/2}$.

Table 2. Selected bond lengths (Å) and angles (°) for **1** and **2**.

Compound **1**			
Eu1–O4	2.333(3)	Eu1–O6	2.372(3)
Eu1–O5^i	2.376(3)	Eu1–O1	2.454(4)
Eu1–O3^i	2.500(3)	Eu1–O2	2.513(3)
Eu1–N1	2.570(4)	Eu1–N2	2.633(4)
Eu1–O4^i	2.591(3)	O4–Eu1–O5^i	75.59(11)
O4–Eu1–O6	74.88(11)	O4–Eu1–O1	91.43(12)
O6–Eu1–O1	129.56(12)	O4–Eu1–O3^i	123.37(11)
O5^i–Eu1–O3^i	92.08(12)	O4–Eu1–N1	141.59(12)
O5^i–Eu1–N1	140.06(12)	O1–Eu1–N1	82.55(13)
O4–Eu1–N2	151.28(12)	O5^i–Eu1–N2	77.57(12)
O1–Eu1–N2	75.10(13)	N1–Eu1–N2	62.81(12)
Compound **2**			
Tb1–N1	2.545(4)	Tb1–N2	2.618(4)
Tb1–O4	2.316(3)	Tb1–O6	2.344(3)
Tb1–O1	2.432(3)	Tb1–O2	2.501(3)
Tb1–O5^i	2.346(3)	Tb1–O3^i	2.473(3)
Tb1–O4^i	2.573(3)	O4–Tb1–O6	75.30(11)
O4–Tb1–O5^i	75.87(11)	O6–Tb1–O5^i	136.70(11)
O4–Tb1–O1	90.96(12)	O4–Tb1–O3^i	123.49(11)
O1–Tb1–O2	52.61(12)	O3^i–Tb1–O2	142.80(12)
O4–Tb1–N1	141.13(11)	O6–Tb1–N1	79.15(11)
O1–Tb1–N1	83.11(13)	O4–Tb1–N2	150.96(12)
O6–Tb1–N2	133.06(12)	O1–Tb1–N2	75.21(12)
O2–Tb1–N2	113.01(12)	N1–Tb1–N2	63.53(12)

Symmetry code: $^i = -x, -y, 2 - z$.

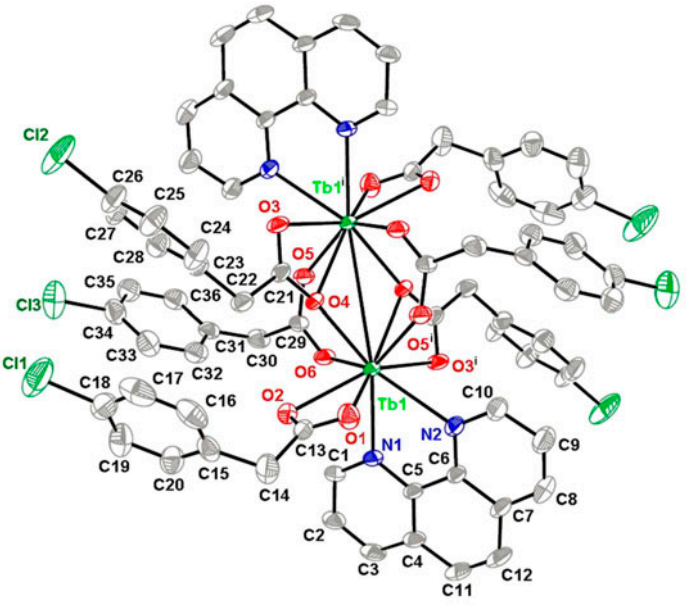

Figure 1. A thermal ellipsoid plot of **2** with 30% probability thermal ellipsoids. All hydrogens are omitted for clarity.

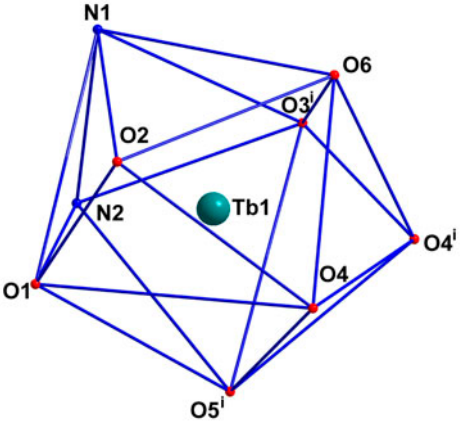

Figure 2. Tricapped trigonal prismatic (TTP) geometry of the Tb(III) of **2** (symmetry code: i = −*x*, −*y*, 2 − *z*).

3. Results and discussion

3.1. *Structure description*

Crystallographic analysis revealed that both **1** and **2** crystallize in the triclinic system, space group *P-1*. Since **1** and **2** are isostructural, only the structure of **2** will be discussed, and a thermal ellipsoid plot of **2** is shown in figure 1. The structure consists of a centrosymmetric

dimer of Tb^{3+} bridged by two bidentate and two tridentate carboxylates. Each Tb(III) is nine-coordinate by seven oxygens of five different 4-cpa$^-$ ligands and two nitrogens of a phen. The metal centers can be described as having distorted tricapped trigonal prismatic geometries (figure 2). O2, O3^i, O4, O5^i, O6, and N2 form the prism and O1, O4^i, and N1 cap the rectangular faces (symmetry code: i = $-x$, $-y$, $2-z$). The dihedral angles between the rectangular faces are 74.12(7)°, 104.14(6)°, and 106.68(5)°. The two Tb–N bond lengths are 2.545(4) and 2.618(4) Å for N1 and N2, respectively. The Tb–O bond distances range from 2.316(3) to 2.573(3) Å and are within the range of those observed for other nine-coordinate Tb(III) complexes with nitrogen and oxygen donors [24, 25]. The lengths of Tb–O bond distances are dependent on coordination of 4-cpa$^-$. The 4-cpa$^-$ ligands in **2** display three coordination modes. One mode is a conventional μ_2-bidentate bridge, bonding to Tb1 through O6 and Tb1^i through O5^i [scheme 1(a)]. The second one is a μ_2-tridentate bridge, chelated to Tb1 through O3^i, and O4^i, with O4^i also linked to Tb1^i [scheme 1(b)]. The third mode is just chelated to Tb1 through O1 and O2 [scheme 1(c)]. The average Tb–O bond lengths for each of these coordination modes are 2.345 (bridging), 2.454 (tridentate), and 2.466 Å (chelating). This indicates that the order of ring strain is chelating > tridentate > bridging. The corresponding M–O bond lengths in $[Gd(2,4\text{-dcp})_3(H_2O)\cdot 2DMF]_n$ (**a**, 2,4-dcp$^-$ = 2,4-dichlorophenoxyacetate) and $[Ce(O_2CCH_2CHMe_2)_3(EtOH)_2]_n$ ($O_2CCH_2CHMe_2$ = isovalerate), both of which show the same carboxylate coordination modes as in **2**, are 2.395, 2.507, 2.523, and 2.405, 2.581, 2.601 Å, respectively [26, 27]. However, in these literature examples, the bridging mode [scheme 1(a)] only connects dimers into an infinite chain, essentially different from this mode in **2**.

The coordination modes of 4-cpa$^-$ in **2** can be compared to other reported compounds involving carboxylates and lanthanide metals. The two coordination modes illustrated in scheme 1(a) and (b) are found in $[Eu(pcpa)_3(H_2O)]_n$ (pcpa$^-$ = 4-chlorophenoxyacetate) [28] and $[Eu(2,4\text{-dcp})_2(phen)_2]_2(ClO_4)_2$ (**b**) [29], while those shown in scheme 1(b) and (c) are found in $[Ln(pcpa)_3(glycol)]_n$ (**c**; Ln = La, Nd, Gd) [30] and $[Nd(2,4\text{-dcp})_3(H_2O)]_n$ [31]. Only one coordination mode, the bridging mode in scheme 1(a), is found in $[\{Er(CCl_3CO_2)_2(H_2O)\}_2(CCl_3CO_2)_2(H_2O)]_n\cdot nH_2O$ ($CCl_3CO_2^-$ = trichloroacetate) [32] and $[La(Ben)_3(Pno)_{0.5}H_2O]$ [33] (Ben = benzoate, Pno = pyridine N-oxide). The Tb···Tb separation (3.973 Å) in **2** just exceeds the sum of the two ionic radii. The short separation may be attributed to combination of bidentate and tridenate bridging carboxylates between the two Tb(II) ions. For **a**, the Gd–Gd distance is 4.255 Å, while for **c**, the Ln–Ln distances are all

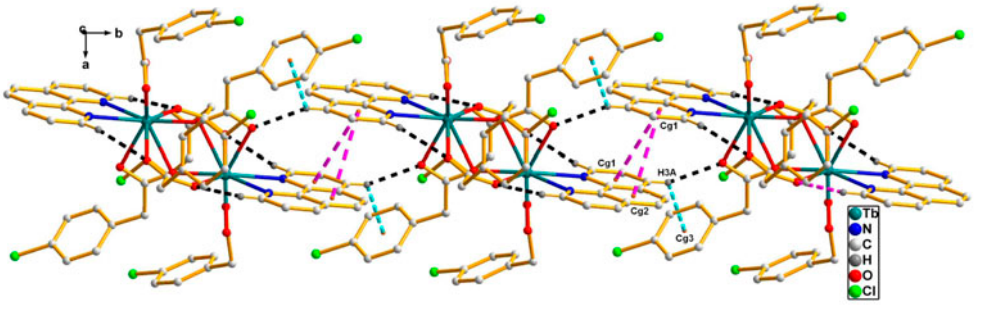

Figure 3. View of the 1-D infinite chain of **2** formed by C3–H3A···O3 hydrogen bonds (black dashed lines), C3–H3A···π (turquoise dashed lines) and $\pi\cdots\pi$ stacking interactions (pink dashed lines, see http://dx.doi.org/10.1080/00958972.2014.904042 for color version).

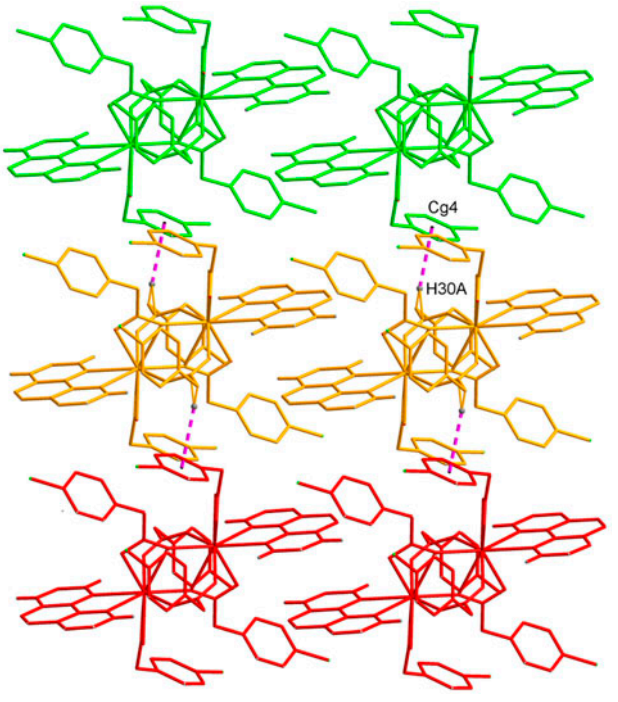

Figure 4. View of 2-D layered network of **2** through C30–H30A···π stacking interactions (pink dashed lines, see http://dx.doi.org/10.1080/00958972.2014.904042 for color version).

greater than 4.215(3) Å. For **b**, which also has bidentate and tridendate carboxylates bridging the Eu centers, the Eu–Eu separation is 4.0357 Å.

The centrosymmetric dinuclear molecules are further connected into 1-D infinite chains through intermolecular C3–H3A···O3 hydrogen bonding interactions, $\pi\cdots\pi$, and C3–H3A···π stacking interactions. The centroid–centroid distances involving parallel pyridine rings (Cg1=N1/C1–C5 ring) of neighboring phen ligands, and between the pyridine ring (Cg1) and the benzene ring (Cg2=C4–C11 ring) of neighboring phen ligands are 3.750 (2) and 3.789(4) Å, respectively. The H–centroid distance H3A···Cg3^{ii} (Cg3=C23–C28 ring) is 2.904(3) Å (figure 3). Adjacent chains are further connected into a 2-D layered network through C30–H30A···π stacking interactions, with a H30A···Cg4^{ii} (Cg4=C15–C20 ring) of 2.952(5) Å (figure 4). Moreover, intramolecular C–H···O hydrogen bonds are also observed.

There are only small differences between the crystal structures of **1** and **2**. Table 2 shows that corresponding bond lengths decrease from **1** to **2**, in accord with the decrease of the metal radius, leading to a decrease of the cell volume (table 1); this is consistent with the well-known lanthanide contraction.

3.2. *Powder X-ray diffraction analysis*

In order to check the purity of **1** and **2**, bulk samples were measured by X-ray powder diffraction at room temperature. As shown in figure 5, the peak positions of the experimental

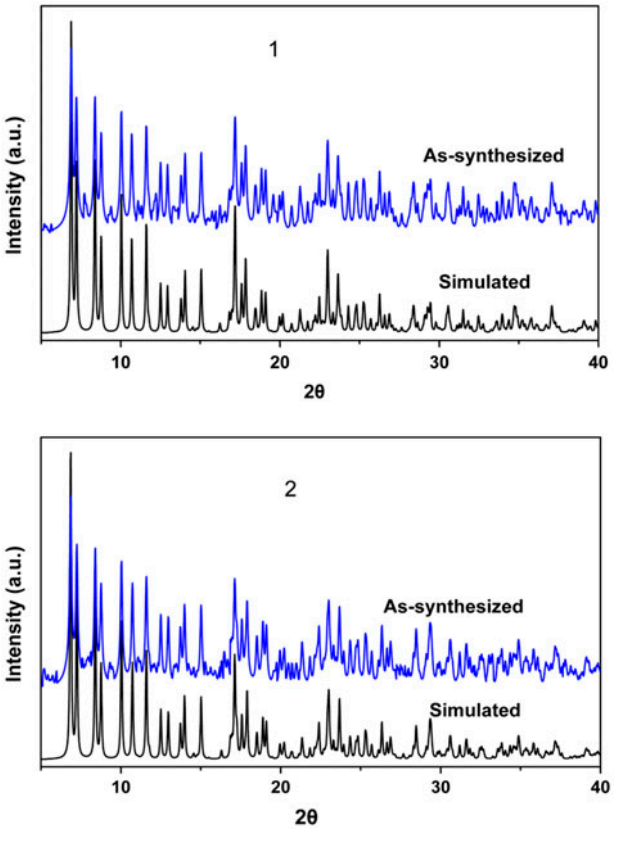

Figure 5. Experimental and simulated PXRD patterns of **1** and **2**.

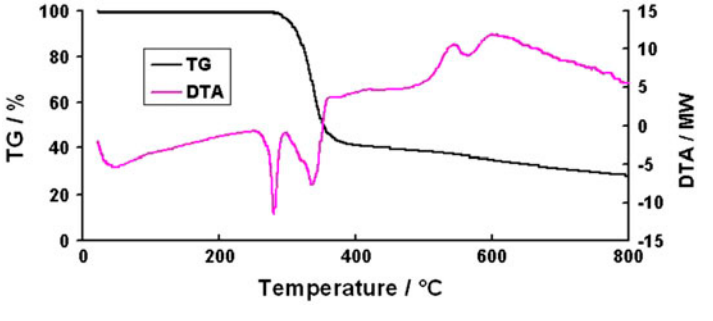

Figure 6. TGA and DTA curves of **2**.

patterns are in agreement with the simulated patterns from the single-crystal data, which clearly indicates good phase purity of the complexes.

3.3. *Infrared spectra*

In the IR spectra of **1** and **2** (figure S1 see online supplemental material at http://dx.doi.org/10.1080/00958972.2014.904042), peaks at 1609, 1560, and 1493 cm^{-1} for **1**, and 1611, 1557, and 1492 cm^{-1} for **2** are associated with the asymmetric and symmetric stretches of the carboxylates. The respective values of ($v_{asym}(COO^-)v_{sym}(COO^-)$) suggest that the carboxylates adopt two coordination modes, in agreement with the observed X-ray structure [34].

3.4. *TG analyses*

The TGA of **1** and **2** indicated that they decomposed to give Eu_2O_3 and Tb_2O_3 as end products. As shown in figure 6, **2** exhibits thermal stability as no clean weight loss occurs below 300 °C. A continuous weight loss occurred above 300 °C which corresponds to decomposition of the framework structure. Finally, **2** was completely degraded to Tb_2O_3 with total loss of 78.12 wt% (Calcd 78.39 wt%). The TGA curve of **1** showed that it had a similar thermal stability (figure S2), further indicating their isostructural architectures.

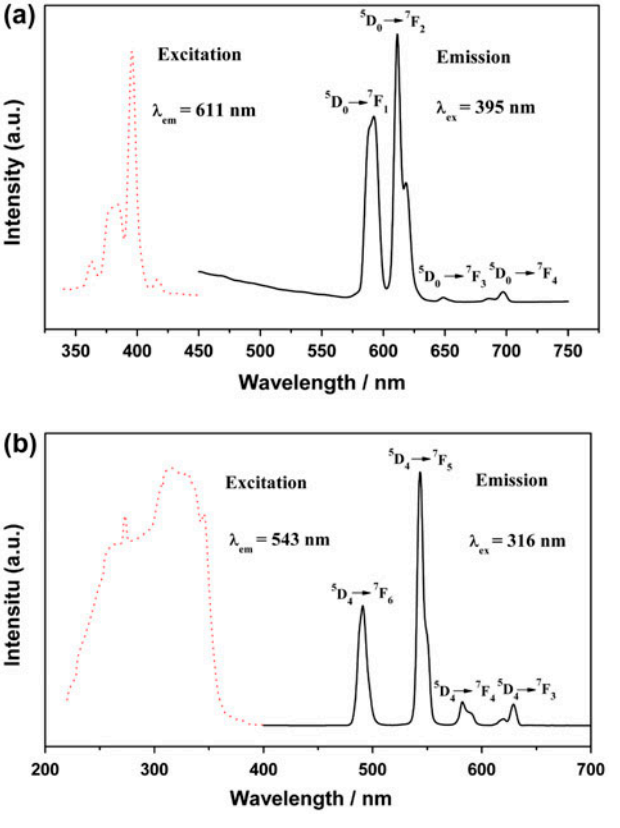

Figure 7. Room temperature fluorescence spectra of **1** (a) and **2** (b) under excitation at 395 and 316 nm, respectively.

3.5. *Luminescent properties*

Metal–organic hybrid coordination polymers with lanthanides have been widely investigated for fluorescence. Lanthanides only exhibit weak emissions under direct excitation due to their low molar absorptivity. Lanthanide-centered emissions can be sensitized by coordination of organic ligands with π-systems, which can efficiently absorb and transfer the energy. The room temperature solid-state excitation and emission luminescence spectra of **1** and **2** are shown in figure 7. The excitation spectrum for **1** showed a band centered at 395 nm. The emission spectrum of **1** revealed the characteristic intense red emission of Eu, attributed to $^5D_0 \rightarrow {}^7F_n$ ($n = 1 \rightarrow 4$) transitions at 592, 611, 649, and 697 nm. The emission at 611 nm is characteristic of the hypersensitive $^5D_0 \rightarrow {}^7F_2$ transition of Eu^{III}, which is much more intense than the $^5D_0 \rightarrow {}^7F_1$ transition at 592 nm. The intensity ratio I ($^5D_0 \rightarrow {}^7F_2/{}^5D_0 \rightarrow {}^7F_1$) is equal to ca. 1.44, which further confirms that Eu(III) ions have a low symmetry coordination environment [35]. As shown in figure 7(b), there are four main peaks in the emission spectrum of **2** with an excitation wavelength at 316 nm. These are ascribed to characteristic emissions of Tb(III) and correspond to electronic transitions from the emitting level $^5D_4$ to the ground multiplet ^7F_n ($n = 6 \rightarrow 3$) [36]. The most intense emission at 543 nm corresponds to the $^5D_4 \rightarrow {}^7F_5$ transition. The second-most intense emission at 491 nm corresponds to the $^5D_4 \rightarrow {}^7F_6$ transition. Bands at 582 and 628 nm correspond to the $^5D_4 \rightarrow {}^7F_4$ and $^5D_4 \rightarrow {}^7F_3$ transitions, respectively. The solid-state emission spectra of **1** and **2** are clearly red shifted compared with free 4-Hcpa and phen (figure S3). This can be attributed to interaction between the lanthanide ions and ligands. Interestingly, **1** and **2** possess long fluorescence lifetimes ($\tau = 0.890$ ms for **1** at 611 nm; 0.995 ms for **2** at 543 nm) (figure 8).

To gain a better understanding of the luminescence efficiency of **2**, the overall quantum yields were calculated. The absolute quantum yield ($\Phi_{overall}$) for a lanthanide complex treats the system as a "black box" in which the internal process is not considered explicitly. Given that the complex absorbs a photon (i.e. the antenna is excited), the overall quantum yield can be defined as follows [37]:

$$\Phi_{overall} = \Phi_{sen}\Phi_{Tb} \quad (1)$$

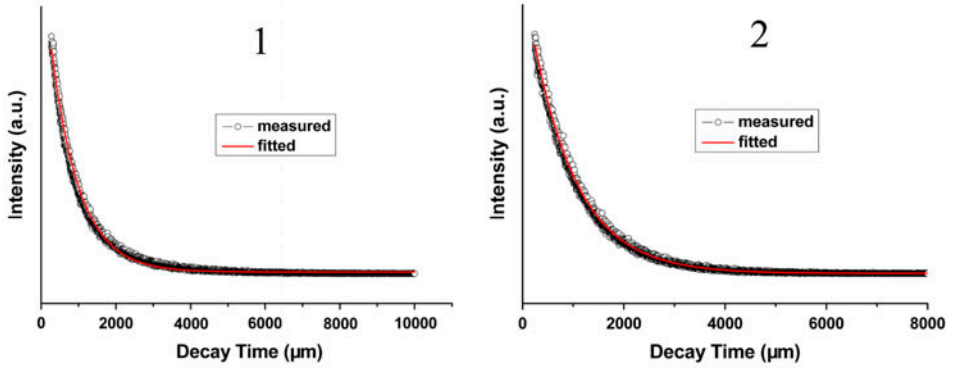

Figure 8. Luminescent lifetimes for **1** (a) and **2** (b).

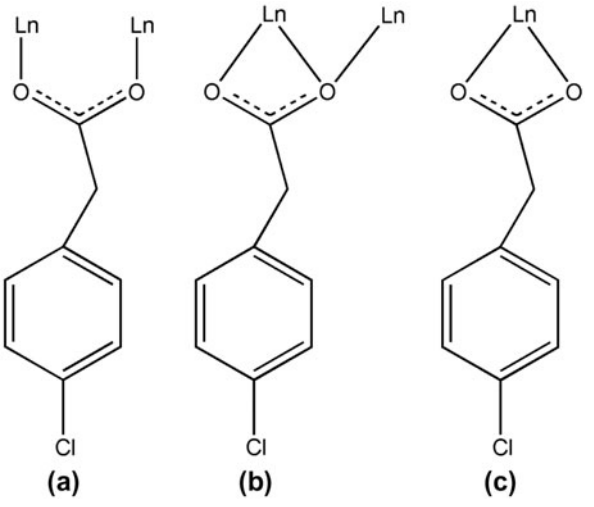

Scheme 1. The coordination modes of 4-cpa$^-$ in **1** and **2**.

Table 3. The $^5D_4$ lifetime (τ_{obs}), radiative lifetime (τ_{RAD}), intrinsic quantum yield (Φ_{Tb}), energy transfer efficiency (Φ_{sen}), and overall quantum yields ($\Phi_{overall}$) for **2**.

τ_{obs}/μs	τ_{RAD}/μs	Φ_{Tb} (%)	Φ_{sen} (%)	$\Phi_{overall}$ (%)
995 ± 0.8	1012 ± 0.8	98	0.37	0.35

Here, Φ_{sen} represents the efficiency of the energy transfer from the ligand to the Tb^{3+} ion and Φ_{Tb} represents the intrinsic quantum yield of Tb^{3+}, which can be calculated from the following equation:

$$\Phi_{Tb} = (A_{RAD}/(A_{RAD} + A_{NR})) = \tau_{obs}/\tau_{RAD} \quad (2)$$

The intrinsic quantum yield for Tb^{3+} (Φ_{Tb}) was estimated by means of equation (3) with the assumption that the decay process at 77 K in a deuterated solvent is purely radiative [38].

$$\Phi_{Tb} = \tau_{obs(298\,K)}/\tau_{RAD(77\,K)} \quad (3)$$

Table 4. Herbicidal activities of 4-Hcpa, **1**, **2** and quizalofop-P-ethyl.

	Inhibitory rate (%)					
	B. napus L.			*E. crusgalli* L.		
Compounds	100 ppm	50 ppm	10 ppm	100 ppm	50 ppm	10 ppm
4-Hcpa	32.1	26.2	10.6	92.4	86.2	41.9
1	35.9	30.8	14.3	95.3	90.7	46.2
2	36.4	29.7	15.1	96.1	91.2	45.7
Quizalofop-P-ethyl	52.3	40.2	32.5	100	94.3	61.2

The overall absolute yield ($\Phi_{overall}$), intrinsic quantum yield (Φ_{Tb}), and energy transfer efficiency (Φ_{sen}) for **2** are presented in table 3. In the solid state, the overall quantum yield for **2** was determined according to the absolute method of de Mello *et al.* [39]. The poor luminescence efficiency ($\Phi_{overall} < 0.1$) of **2** may be due to the weak sensitization efficiency ($\Phi_{sen} = 0.038\%$) of 4-cpa$^-$ with respect to Tb^{3+}.

3.6. *Biological activity*

The herbicidal activities of 4-Hcpa, **1** and **2** were investigated as shown in table 4. Compared to the activities of quizalofop-P-ethyl, the rates of inhibition of *B. napus* L. root growth of the three tested compounds were 32.1–36.4, 26.2–30.8, and 10.6–15.1% at concentrations of 100, 50, and 10 ppm, respectively, which means that the 4-Hcpa, **1** and **2** displayed low herbicidal activities against this plant. However, the rates of inhibition of *E. crusgalli* L. root growth were high (92.4–96.1%) at a concentration of 100 ppm, 86.2–91.2% at 50 ppm, and 41.9–46.2% at 10 ppm, and these activities were close to those for quizalofop-P-ethyl. The results revealed that 4-Hcpa, **1** and **2** exhibited excellent herbicidal activities against this kind of weed at 100 and 50 ppm, but their activities were not satisfactory at the lowest concentration (10 ppm). The complexes showed superior activity to 4-Hcpa. It is possible that 4-Hcpa may be activated by Ln^{3+} [40]. Jiang and co-workers synthesized ten 4-(4,6-dimethoxypyrimidin-2-yloxy)phenoxy acetates and 4-(4,6-dimethylpyrimidin-2-yloxy)phenoxy acetates, and the rates of inhibition of *B. napus* L. root growth were 15.9–58.4, 13.1–36.4, and 9.2–22.9% at concentrations of 100, 50, and 10 mg/L, respectively [41]. Morita *et al.* synthesized a new compound of α-thujaplicin [42]. Its growth-inhibitory activity against *B. campestris* L. was as high as those of other hinokitiol-related compounds, and it completely inhibited the germination of the seeds of *E. utilis* even at 10 ppm. Kapoor *et al.* synthesized several lanthanide complexes with 3-formyl-4-chlorocoumarin hydrazinecarbothioamide and 3-formyl-4-chlorocoumarin hydrazinecarboxamide, which showed pesticidal, nematicidal, antibacterial, and antifungal activities [7]. Shen *et al.* reported five lanthanide complexes based on 2-thenoyltrifluoroacetone and *p*-hydroxybenzoic acid. The antibacterial activities showed that the Er complex had superior antibacterial ability against *E. coli* and *S. aureus*, with diameter of growth inhibition area of 22 and 23 m and a MIC of 100 and 120 μg/mL [8]. Compared to these reported compounds, 4-Hcpa, **1** and **2** show good activities against *E. crusgalli* L. However, until now, work on the study of herbicidal activity of lanthanide complexes based on aromatic carboxylic acids has not been reported.

4. Conclusion

We have synthesized and structurally characterized two new isostructural dinuclear lanthanide complexes based on 4-cpa$^-$ and phen. Both **1** and **2** emit intense luminescence with long fluorescence lifetimes of 0.890 ms (at 611 nm) and 0.995 ms (at 543 nm), respectively. The poor sensitization observed for **2** may mainly be due to the weak sensitization efficiency ($\Phi_{sen} = 0.040\%$) of 4-Hcpa with respect to Tb^{3+}. 4-Hcpa, **1** and **2** were tested as herbicides, and the preliminary bioassay indicated that the ligand and complexes exhibited high herbicidal activities against monocotyledonous plants such as *E. crusgalli* L. at concentrations of 100 and 50 ppm.

Supplementary material

IR spectra of **1** and **2**; TGA and DTA curves for **2**; room temperature emission spectra for 4-Hcpa and phen. Crystallographic data for the structures reported in this article have been deposited with the Cambridge Crystallographic Data Center, CCDC No. 921904 and 921905. Copies of this information may be obtained free of charge from the Director, CCDC, 12 Union Road, Cambridge, CB21EZ, UK (Fax: +44 1223 336 033; E-mail: deposit@ccdc.cam.ac.uk or (http://www.ccdc.cam.ac.uk) or also available from the author on request.

Funding

This work was partially supported by Natural Science Research Foundation of Zhaoqing University, China [grant number 201003]; Educational Research Foundation of Zhaoqing University, China [grant number JY201154]; Foundation for Distinguished Young Talents in Higher Education of Guangdong Province [grant number 2012LYM_0134]; Science and Technology Planning Project of Zhaoqing City [grant number 2012G013]; China Natural Science Fund [grant number 81202461]; and the China Postdoctoral Science Foundation [grant number 2013M531906].

References

[1] J.P. Galdwell, W. Henderson, N.D. Kim. *J. Forensic Sci.*, **46**, 1332 (2001).
[2] H. Tsukube, S. Shinoda. *Chem. Rev.*, **102**, 2389 (2002).
[3] D. Ma, W. Wang, Y. Li, J. Li, C. Daiguebonne, G. Calvez, O. Guillou. *CrystEngComm*, **12**, 4372 (2010).
[4] J. Kido, Y. Okamoto. *Chem. Rev.*, **102**, 2357 (2002).
[5] N. Marques, A. Sella, J. Takats. *Chem. Rev.*, **102**, 2137 (2002).
[6] M. Bortoluzzi, G. Paolucci, D. Fregona, L.D. Via, F. Enrichi. *J. Coord. Chem.*, **65**, 3903 (2012).
[7] P. Kapoor, R.V. Singh, N. Fahmi. *J. Coord. Chem.*, **65**, 262 (2012).
[8] Z. Shen, D. Xu, N. Cheng, X. Zhou, X. Chen, Y. Xu, Q. He. *J. Coord. Chem.*, **64**, 2342 (2011).
[9] Y.C. Liang, R. Cao, W.P. Su, M.C. Hong, W.J. Zhang. *Angew. Chem. Int. Ed.*, **39**, 3304 (2000).
[10] K.P. Mörtl, J.P. Sutter, S. Golhen, L. Ouahab, O. Kahn. *Inorg. Chem.*, **39**, 1626 (2000).
[11] A. Jana, S. Majumder, L. Carrella, M. Nayak, T. Weyhermueller, S. Dutta, D. Schollmeyer, E. Rentschler, R. Koner, S. Mohanta. *Inorg. Chem.*, **49**, 9012 (2010).
[12] R. Koner, G.H. Lee, Y. Wang, H.H. Wei, S. Mohanta. *Eur. J. Inorg. Chem.*, **2005,** 1500 (2005).
[13] D.Y. Ma, H.F. Guo, L. Qin, Y. Pan, K. Lu, J.Q. Liu. *J. Coord. Chem.*, **65**, 3424 (2012).
[14] M. Iqbal, I. Ahmad, S. Ali, N. Muhammad, S. Ahmed, M. Sohail. *Polyhedron*, **50**, 524 (2013).
[15] K. Rauf, M. Bolte. *Private Commun.* (2010). Available online at: http://www.ccdc.cam.ac.uk/services/structure_deposit
[16] B.K. Shah, D.C. Neckers, J. Shi, E.W. Forsythe, D. Morton. *Chem. Mater.*, **18**, 603 (2006).
[17] N.S. Kumar, S. Varghese, N.P. Rath, S. Das. *J. Phys. Chem. C*, **112**, 8429 (2008).
[18] S.V. Eliseeva, O.V. Kotova, F. Gumy, S.N. Semenov, V.G. Kessler, L.S. Lepnev, J.C.G. Bünzli, N.P. Kuzmina. *J. Phys. Chem. A*, **112**, 3614 (2008).
[19] L.Y. Mu. *Research Method of Plant Chemical Protection*, pp. 90–91, China Agriculture Press, Beijing (1994).
[20] B.L. Wang, R.G. Duggleby, Z.M. Li, J.G. Wang, Y.H. Li, S.H. Wang, H.B. Song. *Pest Manage. Sci.*, **61**, 407 (2005).
[21] Bruker. *APEXII Software (Version 6.3.1)*, Bruker AXS Inc., Madison, WI, USA (2004).
[22] S. Parkin, B. Moezzi, H. Hope. *J. Appl. Crystallogr.*, **28**, 53 (1995).
[23] G.M. Sheldrick. *Acta Crystallogr., Sect. A: Found. Crystallogr.*, **64**, 112 (2008).
[24] B. Barja, P. Aramendia, R. Baggio, M.T. Garland, O. Peña, M. Perec. *Inorg. Chim. Acta*, **355**, 183 (2003).
[25] A.Y. Fu, Y.P. Wu, F.M. Wang, Y.L. Sun. *J. Coord. Chem.*, **63**, 3724 (2010).
[26] C. Dendrinou-Samara, D. Drosou, L. Iordanidis, A. Terzis, D.P. Kessissoglou. *J. Inorg. Biochem.*, **92**, 156 (2002).
[27] I.L. Malaestean, M. Kutluca-Alıcı, A. Ellern, J. van Leusen, H. Schilder, M. Speldrich, S.G. Baca, P. Kögerler. *Cryst. Growth Des.*, **12**, 1593 (2012).

[28] R.Q. Sun, H.H. Zhang, Y.N. Cao, Y.P. Chen, Z. Wang, Q.Y. Yang. *Chinese J. Struct. Chem.*, **25**, 844 (2006).
[29] S.M. Shi, Z.F. Chen, Y.C. Liu, L. Mao, H. Liang, Z.Y. Zhou. *J. Coord. Chem.*, **61**, 2725 (2008).
[30] Z. Wang, D.S. Liu, H.H. Zhang, C.C. Huang, Y.N. Cao, X.H. Yu. *J. Coord. Chem.*, **61**, 419 (2008).
[31] J. Guo, W.J. Liang, W.D. Song. *Acta Cryst.*, **E63**, m1595 (2007).
[32] T. Imai, A. Ouchi. *Bull. Chem. Soc. Jpn.*, **60**, 408 (1987).
[33] R. Sarma, J.B. Baruah. *J. Coord. Chem.*, **63**, 457 (2010).
[34] K. Nakamoto. *Infrared and Raman Spectra of Inorganic and Coordination Compounds*, 4th Edn, Wiley, New York (1986).
[35] J.C.G. Bünzli. In *Lanthanide Probes in Life, Chemical and Earth Sciences, Theory and Practice*, J.C.G. Bünzli, G.R. Choppin (Eds), Chap. 7, Elsevier Scientific Publishers, Amsterdam, The Netherlands (1989).
[36] B. Zhao, X.Y. Chen, P. Cheng, D.Z. Liao, S.P. Yan, Z.H. Jiang. *J. Am. Chem. Soc.*, **126**, 15394 (2004).
[37] M. Xiao, P.R. Selvin. *J. Am. Chem. Soc.*, **123**, 7067 (2001).
[38] S. Biju, M.L.P. Reddy, A.H. Cowley, K.V. Vasudevan. *J. Mater. Chem.*, **19**, 5179 (2009).
[39] J.C. de Mello, H.F. Wittmann, R.H. Friend. *Adv. Mater.*, **9**, 230 (1997).
[40] O.E. Offiong, E. Nfor, A.A. Ayi. *Transition Met. Chem.*, **25**, 369 (2000).
[41] L. Jiang, H. Wang, M. Wang, X. Teng. *Molecules*, **15**, 1074 (2010).
[42] Y. Morita, E. Matsumura, H. Tsujibo, M. Yasuda, Y. Sakagami, T. Okabe, N. Ishida, Y. Inamori. *Biol. Pharm. Bull.*, **24**, 607 (2001).